Low-Temperature Control of Nanoscale Morphology for High Performance Polymer Photovoltaics

ARTICLE *in* NANO LETTERS · NOVEMBER 2008

Impact Factor: 13.59 · DOI: 10.1021/nl802425r · Source: PubMed

8 AUTHORS, INCLUDING:

Justin M Hodgkiss
Victoria University of Wellington
62 PUBLICATIONS **1,877** CITATIONS
SEE PROFILE

Sebastian Westenhoff
University of Gothenburg
39 PUBLICATIONS **1,511** CITATIONS
SEE PROFILE

Ian A Howard
Karlsruhe Institute of Technology
51 PUBLICATIONS **2,203** CITATIONS
SEE PROFILE

Christopher R. McNeill
Monash University (Australia)
112 PUBLICATIONS **3,794** CITATIONS
SEE PROFILE

NANO
LETTERS

XXXX
Vol. xx, No. x
-

Low-Temperature Control of Nanoscale Morphology for High Performance Polymer Photovoltaics

Andrew R. Campbell,† Justin M. Hodgkiss,† Sebastian Westenhoff,‡ Ian A. Howard,† Robert A. Marsh,† Christopher R. McNeill,† Richard H. Friend,† and Neil C. Greenham*,†

Optoelectronics Group, Cavendish Laboratory, Department of Physics, University of Cambridge, CB3 0HE, U.K., and Department of Chemistry, Biochemistry and Biophysics, University of Gothenburg, 40530 Gothenburg, Sweden

Received August 9, 2008; Revised Manuscript Received October 2, 2008

ABSTRACT

Understanding and controlling nanoscale morphology is crucial to the performance of polymer bulk heterojunction solar cells, as well as other optoelectronic devices such as polymer light-emitting diodes, field-effect transistors, and sensors. In photovoltaic devices, optimum blend morphologies must be commensurate with the nanometer length scales of exciton diffusion and charge separation. We report on a generally applicable method of optimizing the phase segregation in polymer−polymer bulk heterojunctions based on tuning mixtures of low and high boiling point solvents. We have characterized the resulting blend morphologies with nanometer resolution using a transient absorption technique that probes the distribution of paths traveled by the excitons themselves prior to generating charges at an interface. Photovoltaic efficiencies are accounted for in terms of exciton diffusion, geminate pair separation, and polymer ordering, all of which are sensitive to the nanoscale morphology determined by the composition of the solvent mixture.

Organic photovoltaics have been the subject of extensive investigation due to their potential for economically viable solar energy conversion.[1,2] In these low-permittivity systems, photogenerated excitons are dissociated into charges only upon diffusion to a donor−acceptor interface, and the resultant geminate electron−hole pairs must then overcome their mutual Coulombic attraction in order to be separated and collected at the electrodes. The highest efficiency polymer−polymer[3] and polymer−fullerene[4] devices employ bulk heterojunction architectures consisting of intimately mixed electron donor and acceptor materials. A bulk heterojunction architecture results when the donor−acceptor mix is deposited from a common solvent with some degree of enthalpically driven demixing occurring upon drying. Recent studies on polymer−polymer blend devices have confirmed the importance of the nanoscale phase separation of the binary polymer components.[5,6] Device efficiency is optimized when polymer domains are small enough for efficient migration of excitons to an interface, yet large enough to promote efficient long-range geminate charge separation.

For the full potential of organic photovoltaics as a cost-effective means of energy generation to be realized, efficient scalable manufacturing processes such as roll-to-roll printing must be used.[7] Existing methods of optimizing the nanoscale morphology of bulk heterojunctions such as thermal annealing[8] and solvent annealing[9] add complexity and expense to manufacture. The choice of solvent has long been known to affect the efficiency of polymer bulk heterojunction devices, largely attributed to the morphological evolution during drying.[10] However, solvent choice alone is rarely sufficient for optimum performance. The use of high boiling point solvents can increase phase separation beyond the range of efficient exciton diffusion and compromise the smoothness of thin films resulting in electrical shorting of devices.

Mixtures of solvents have been previously investigated for the manufacture of polymer−fullerene blends. Combining chloroform with chlorobenzene was shown to improve performance by suppressing nongeminate recombination.[11] Recent work on polymer−fullerene bulk heterojunctions has investigated the effect on morphology of processing additives chosen for selective solvation of the fullerene component.[12,13] These additives enhance device performances by preventing isolated fullerene molecules from being dissolved throughout polymer phases.

Here we demonstrate a method of controlling the nanoscale morphology of a polymer−polymer bulk heterojunction by adding a small volume-fraction of a higher boiling point cosolvent to the polymer blend solution. By using a majority

* To whom correspondence should be addressed.
† University of Cambridge.
‡ University of Gothenburg.

10.1021/nl802425r CCC: $40.75
Published on Web 10/25/2008

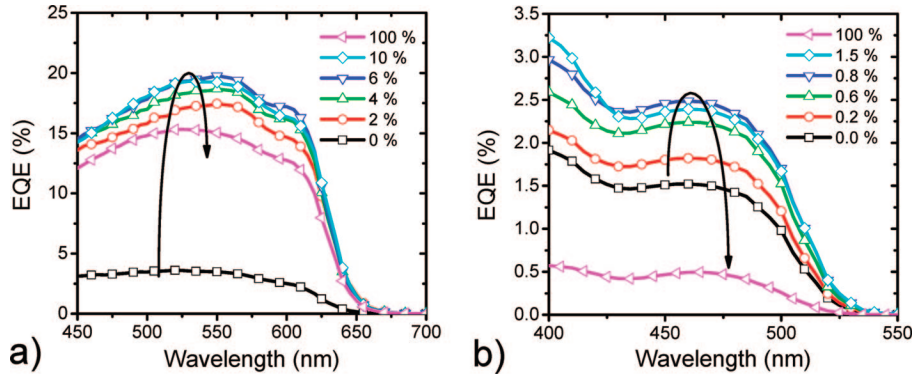

Figure 1. Spectral response of the external quantum efficiency (EQE) of (a) P3HT−F8TBT and (b) PFB−F8BT photovoltaic devices spun from a mixture of chloroform with a varying volume-fraction of *p*-xylene.

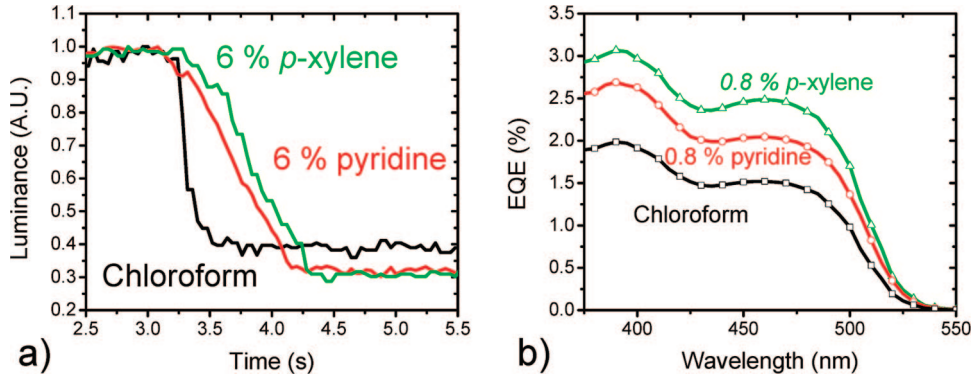

Figure 2. (a) Luminance of a P3HT−F8TBT film during spin coating of a film spun from chloroform alone and with the addition of 6% volume-fraction of pyridine and *p*-xylene. (b) EQE spectra of devices spun from chloroform alone, and with the addition of 0.8% volume-fraction of pyridine and *p*-xylene.

low boiling point solvent macroscopically smooth thin films can be produced. However, with the addition of a small volume fraction of high boiling point cosolvent the morphology can continue to evolve in a solvent-rich environment since both polymer pairs show high solubility in both solvents. The morphology can be defined with precision simply by adjusting the ratio of these two solvents. The optimized nanoscale morphology of these solar cells was too small to image directly using atomic force microscopy. The effect of changing the solvent mixture is investigated using a transient absorption spectroscopic technique whereby the temporally resolved charge generation is analyzed to elucidate the morphology with nanometer spatial resolution.

The systems investigated here are a high performance polythiophene−polyfluorene blend,[3] poly((9,9-dioctylfluorene)-2,7-diyl-alt-[4,7-bis(3-hexylthien-5-yl)-2,1,3-benzothiadiazole]-2,2-diyl) (F8TBT) with poly(3-hexylthiophene) (P3HT) and a well-characterized polyfluorene blend,[14−16] poly(9,9-dioctylfluorene-co-benzothiadiazole) (F8BT) with poly(9,9-dioctylfluorene-co-bis-N,N′-(4,butylphenyl)-bis-N,N′-phenyl-1,4-phenylene-diamine) (PFB). The manufacture of these devices is described in the Device Fabrication section.

Figure 1 shows the external quantum efficiency (EQE) spectra of devices spun from chloroform solutions with the addition of *p*-xylene. All of the polymers used in this investigation are known to have high solubility in both chloroform and *p*-xylene, which have disparate boiling points of 61 and 138 °C, respectively. EQE spectra were determined by illuminating through the semitransparent electrode of the devices with a quartz-halogen lamp via a monochromator and measuring the short-circuit current using a Keithley Instruments 237 source measure unit. The light incident on the devices (∼1 mW/cm^2) was measured using a beam splitter and a calibrated Si photodiode. In the case of a P3HT−F8TBT device (Figure 1a), the peak EQE increases monotonically from only 3.6% for the chloroform-only device to 19.8% for the device with 6% *p*-xylene. At 10% volume-fraction of *p*-xylene the EQE begins to decrease and a device spun from a pure *p*-xylene solution shows a peak EQE of 15.3%. There is also a pronounced increase in EQE for the PFB−F8BT devices (Figure 1b) at all wavelengths for 0−0.8% volume-fraction of *p*-xylene. However, at 1.5% *p*-xylene the 460 nm peak, which corresponds to absorption in F8BT, begins to decrease while the 390 nm peak, corresponding to PFB absorption is still increasing. A device spun from pure *p*-xylene shows a significantly lower EQE.

Upon spin coating P3HT−F8TBT films, a darkening of their color is strikingly apparent by eye as the film solidifies. This darkening was quantitatively resolved using a CCD camera, as shown in Figure 2a. With the addition of 6% *p*-xylene, the rate of color change in the film is a factor of 2 slower than that of the film spun from chloroform alone. This is evidence that the addition of *p*-xylene to the chloroform solution is increasing the drying time during the final stages of film formation, allowing the nanoscale

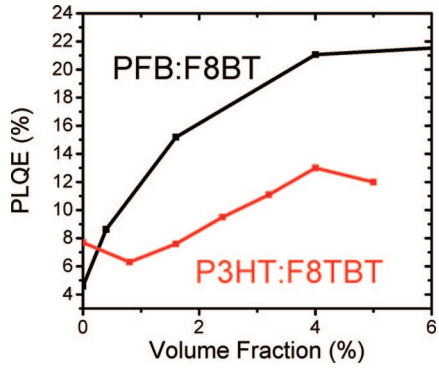

Figure 3. Photoluminescence quantum efficiency (PLQE) of PFB−F8BT (black) and P3HT−F8TBT (red) films spun from a solution of chloroform with a varying volume-fraction of *p*-xylene.

morphology of the film a longer time to evolve in a solvent-rich environment.[17,18] The drying time of a film spun from a solution with 6% pyridine is between that of a film from a chloroform solution and a pyridine solution. Pyridine has a boiling point of 115 °C, between that of chloroform and *p*-xylene. The drying time appears to be related to the boiling point of the cosolvent, even for low volume fractions.

Figure 2b shows the EQE of PFB−F8BT devices spun from chloroform solutions with the addition of 0.8% volume-fraction of pyridine and *p*-xylene. The EQE spectrum of the pyridine processed device falls between those of the device spun from chloroform alone and the device processed with *p*-xylene cosolvent. This is consistent with the hypothesis that in PFB−F8BT devices the device performance is dependent on the boiling points of the solvents in the mixture, rather than the chemical structure of the solvent.

Figure 3 shows the photoluminescence quantum efficiency (PLQE) of both P3HT−F8TBT and PFB−F8BT films prepared from chloroform with varying volume-fractions of *p*-xylene cosolvent. PLQE measurements can be interpreted to assess the efficiency of conversion of emissive excitons to charges. The films were excited with a 488 nm argon-ion laser and PLQE was measured using the integrating sphere method.[19] In both systems, increasing the cosolvent fraction increases the PLQE. In thermal annealing studies of polymer−polymer blends, an increase in PLQE has been shown to correspond to a coarsening of single polymer domains because excitons formed in larger domains can decay radiatively before reaching the heterojunction.[5]

The dependence of PLQE and EQE on solvent composition confirms that the blend morphology on the nanometer length scale relevant to exciton diffusion is crucial to photovoltaic device efficiencies. Since this length scale is too small to be resolved using atomic force microscopy, we have used a transient absorption (TA) technique that probes the migration of the excitons themselves prior to generating charges at an interface. As the photons are absorbed throughout the polymer domains, the distribution of the distances traveled by the resultant excitons to reach a hetrojuction provides a unique probe of the nanometer scale morphology of the blends. In this analysis, recently described by Westenhoff et al.,[20] the distribution of distances that excitons have diffused to encounter a heterojunction can be extracted from the TA dynamics of charge generation provided that TA spectra for excitons and charges can be clearly distinguished and the time-dependent exciton diffusion rate can be independently established. These requirements are readily fulfilled in PFB−F8BT blends, which also have the significant advantage that the lower bandgap material (F8BT) can be selectively excited and initial energy transfer to the lower bandgap material can be excluded from the analysis.

Femtosecond TA measurements were performed on PFB−F8BT films using an experimental setup as described in detail elsewhere.[20] In this experiment, films were pumped with 488 nm pump pulses (fwhm ∼80 fs), selectively exciting the lower bandgap F8BT polymer with the power attenuated to ∼20 nJ/pulse (fluence ∼4×10^{13} photons/cm^2) to avoid nonlinear effects.[16] Excitation was followed by a broadband visible probe pulse, and its differential transmission spectrum from 520−800 nm was recorded on a spectrometer equipped with a diode array. Using this method, we were able to spectrally and temporally resolve the evolution of excitons to charges on the time scale of ∼150 fs to 2 ns. Figure 4a shows TA spectra for a PFB−F8BT film spun from chloroform at early (0.8−10 ps) and late (100−1600 ps) times, which correspond to the signatures of excitons and charges respectively.[21] The three-dimensional (3D) data (absorption versus wavelength versus time) were spectrally integrated from 570 to 630 nm to produce the kinetics plot shown in Figure 4b. This region was selected because it shows the evolution from stimulated emission ($\Delta T/T > 0$) associated with the exciton to induced absorption from the photogenerated charges ($\Delta T/T < 0$).[21] The reduction in long-lived absorption with increasing *p*-xylene volume-fraction shows that excitons are converted to charges with a lower yield, consistent with the PLQE measurement.

Using the analysis described by Westenhoff et al.[20] the distributions of distances that excitons have diffused through F8BT prior to encountering a heterojunction were extracted from the TA dynamics of charge generation. First, the TA kinetics in Figure 4b were plotted as the normalized populations of charges in the films against time, given the known rate of exciton decay to the ground state, Figure 4c. As charge generation in this system is limited by exciton diffusion to the interface,[20] the charge generation times are equivalent to the arrival times of excitons at a heterojunction. Second, a time-dependent exciton diffusion rate was independently determined by applying a Monte Carlo hopping model to the experimentally observed Stokes shift of excitons relaxing through the density of states of F8BT.[20] Finally, by combining the arrival time of excitons at the heterojunction and the rate at which they diffuse, the distribution of rms distances the excitons have traveled in F8BT domains before encountering a heterojunction is found, as shown in Figure 4d. These distributions are a valuable probe of the nanometer scale morphologies experienced by the excitons themselves.

The most pronounced change in the distribution of rms exciton diffusion distances, Figure 4d, is the change in the height of the peak at 0 nm, which can be attributed to

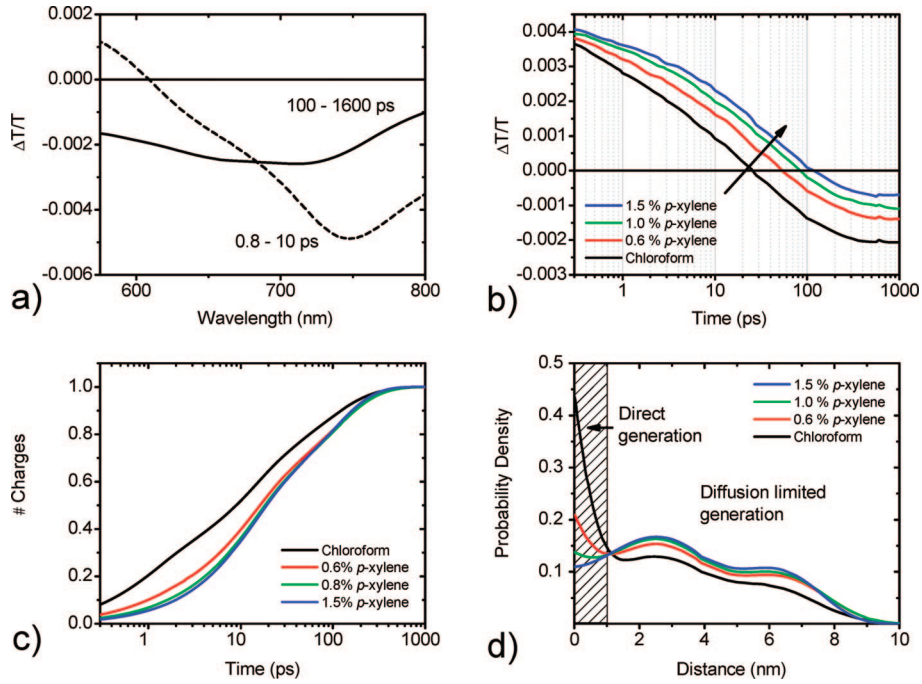

Figure 4. (a) Transient absorption spectra of PFB−F8BT blend films spun from chloroform. (b) Kinetics of PFB−F8BT films spun from chloroform with varying volume fractions of *p*-xylene spectrally integrated over the wavelength range 570−630 nm. (c) Normalized growth of charge population in the above films with time. (d) rms distance traveled by excitons that reached a heterojunction in the above films. These distributions are powerful probe of nanometer scale morphologies.

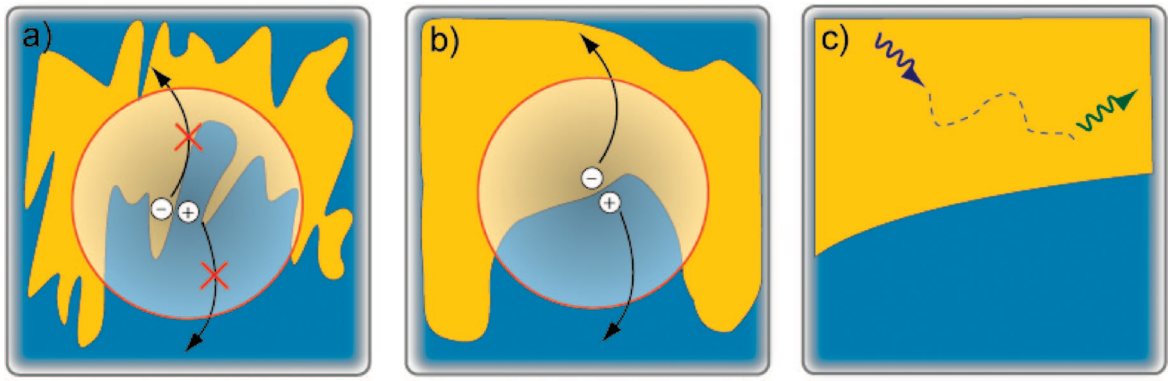

Figure 5. Schematic representation of our key findings. (a) Morphology of a blend spun from a low boiling point solvent only. The high relative interfacial area shown is consistent with the rms distribution measured for charge generation (Figure 4d) in the absence of a colsolvent. Here, charges cannot escape their mutual Coulombic attraction, and recombine. (b) Cosolvent optimized morphology. The measured rms distribution for charge generation shows that the interfacial area is reduced, producing a morphology that balances efficient exciton diffusion and charge separation. (c) High boiling point solvent morphology. Photogenerated excitons decay before they reach a donor acceptor interface.

excitons generated directly at an interface with no diffusion component. The fraction of excitons formed within 1 nm of the interface falls from 26% for a film spun from pure chloroform to 12% for a film with 1.5% volume-fraction of *p*-xylene. The decrease in the fraction of excitons that are generated instantaneously on the heterojunction suggests a decrease in interfacial area of the blend when a higher boiling point cosolvent is added. However, the shape of the distribution of distances traveled by excitons generated in the bulk of the polymer is unchanged; the mean size of polymer domains has not increased. If the size of the domains is the same and the interfacial area is smaller, the edges of the domain must have become smoother. These conclusions are represented schematically in Figure 5.

The changes in film morphology upon cosolvent processing apparent from Figure 4d are consistent with the observed increase in PLQE shown in Figure 3. By combining the PLQE data from Figure 3 and the PLQE of pristine F8BT the efficiency of exciton quenching at the PFB−F8BT interface was calculated. The quenching efficiencies are 94% in the film spun from pure chloroform and 82% in the film from 1.5% *p*-xylene. As observed in Figure 4d the fraction of charge pairs formed from excitons that are absorbed directly on an interface are 26 and 12%, respectively. As excitons absorbed directly on an interface are quenched by definition, the change in exciton quenching observed upon addition of cosolvent (12%) is in good agreement with the change in excitons generated directly at an interface (14%).

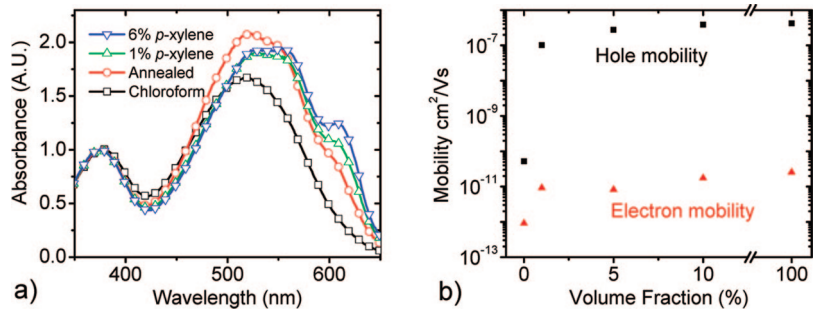

Figure 6. (a) Absorbance spectra of P3HT−F8TBT films spun from chloroform with various processing routes. Samples were spun from pure chloroform (black squares), spun from pure chloroform and thermally annealed (red circles), and spun from chloroform with the addition of 1 and 6% by volume *p*-xylene (blue triangles and green triangles, respectively). (b) Variation of zero-field electron and hole mobility in P3HT−F8TBT diodes spun from chloroform with volume-fraction of *p*-xylene.

As reduction of interfacial area is sufficient to explain the observed increase in PLQE this confirms that the cosolvent is altering the interfacial area of the domains rather their size.

Increased radiative recombination would ostensibly lead to lower photovoltaic efficiencies, yet we observe the opposite. This apparent contradiction is resolved by considering the strong morphological dependence of geminate separation efficiency. Computational models and experimental studies have identified geminate separation as the key determinant of device efficiency in organic bulk heterojunctions.[22−25] In such a system, facile separation occurs when the acceptor and donor domains are coarse enough for the photogenerated charges to move beyond their Coulomb binding radius. When the polymers are too intimately mixed, the percolation of charges away from the interface is hindered. Separation of photogenerated charges is less entropically favorable and geminate recombination prevails.[26−28] By changing the cosolvent ratio in these blends, the morphology of the interface between domains is strongly affected, directly affecting the geminate separation efficiency.

Figure 6a shows the optical absorbance spectra of P3HT−F8TBT films spun from chloroform with a varying volume fraction of *p*-xylene. Also included for comparison is the absorbance spectrum of a P3HT−F8TBT blend that has been thermally annealed. As the volume fraction of cosolvent is increased, the emergence and intensification of a peak at 610 nm is observed. This peak is also observed to a lesser degree in the thermally annealed sample. This spectral feature is attributed to interchain absorption resultant from increased planarization of the P3HT.[29] This absorption has been directly linked to an increase in both the crystallization of the polymer and the efficiency of resultant devices.[30]

Figure 6b shows the change in electron-mobility and hole-mobility of P3HT−F8TBT films spun from chloroform with an increasing volume fraction of *p*-xylene. Because of the strong morphological dependence of the mobility, measurements were made using an electron-only or hole-only diode structure closely resembling that of a photovoltaic device. The dark current under forward bias was measured in these devices using a Keithley Instruments 237 source measure unit and mobility was estimated by fitting the quadratic region to a space-charge limited expression[31]

$$J_{h/e} = \frac{9}{8}\varepsilon_0\varepsilon_r\mu_{h/e}\exp\left(0.891\gamma_{h/e}\sqrt{\frac{V}{L}}\right)\frac{V^2}{L^3}$$

Figure 6b shows an increase of both electron and hole mobilities with increasing cosolvent fraction. The increase in hole mobility is much larger than the increase in electron mobility. This can be attributed to the increase in crystallinity in P3HT observed in the absorption spectra in Figure 6a. F8TBT is amorphous so the small increase in electron mobility is likely to be a morphological change only. The internal quantum efficiency of these blends is known to be limited by the long-range separation of Coulombically bound pairs.[5,25] Increasing the local hole mobility of the P3HT will enhance this separation efficiency,[22] providing an additional route to enhancing the external quantum efficiency of the devices.

In PFB−F8BT blends, there are no changes evident in either the absorption spectra of films or the carrier mobilities of devices. PFB−F8BT blends are amorphous and do not exhibit the evolution of crystalline features observed in P3HT−F8TBT blends. This is consistent with previous work concerning the thermal annealing of this system.[5] The relative increase to the peak EQE achievable with cosolvent processing of the PFB−F8BT devices (1.65-fold increase) is significantly lower than that of the P3HT−F8TBT devices (4.5-fold increase). This is consistent with the conclusion that there is an additional performance enhancement from the increased crystallinity observed in the P3HT. To obtain maximum performance from a polymer blend including a crystalline material, the processing conditions must be chosen not only to optimize domain size for a balance of efficient exciton diffusion and geminate separation but also to maximize the crystallinity.

In conclusion, we have presented a low-temperature processing technique suitable for the manufacture of efficient polymer−polymer blend photovoltaic devices. By controlling the drying time of a polymer film with mixtures of high and low boiling point solvents we have demonstrated control over the extent of phase demixing and crystallinity. For an amorphous bulk heterojunction, performance is optimized when the nanoscale morphology maximizes the product of

exciton diffusion efficiency and geminate charge separation efficiency. Using TA spectroscopy to reveal morphological properties on the nanometer length scale relevant to excitons undergoing charge generation, control of the solvent composition was shown to maximize performance by decreasing the interfacial area of the polymer domains. In a system showing polymer ordering, the use of a high boiling point cosolvent was also shown to enhance the crystallinity beyond that which is observed in a thermally annealed film, with concomitant improvement in the photovoltaic efficiency. A mixture of solvents allows these parameters to be precisely optimized for a wide range of material combinations and is a fast, low-temperature technique suitable for large scale manufacturing processes such as roll-to-roll printing.

Device Fabrication. Blends of PFB/F8BT and P3HT/F8TBT were prepared by dissolving the polymers in chloroform at a concentration of 10 g/L. Both solutions were prepared in the polymer ratio 1:1 by mass. Pyridine and *p*-xylene were added to this solution at a volume-fraction of 0.0−6.0%. The thickness of films were 80 and 110 nm for P3HT/F8TBT and PFB/F8BT, respectively. The thickness did not show a dependence on cosolvent fraction. For comparison, films of the same thickness were spun from pure *p*-xylene solutions at concentrations of 15 g/L for P3HT/F8TBT and 18 g/L for PFB/F8BT. Thin films for optical measurements were prepared by spin-coating the solutions onto quartz substrates. Where required, films were annealed on a hotplate at 140 °C for 10 min immediately after spin-coating.

Photovoltaic devices were prepared by spin-coating the above solutions onto glass substrates prepatterned with a layer of semitransparent indium−tin oxide (ITO). Prior to this deposition the substrates were washed in an ultrasonic bath in acetone and then propan-2-ol, treated in an oxygen-plasma etcher and coated in a 50 nm layer of PEDOT/PSS. Aluminum cathodes were deposited to a thickness of 100 nm by thermal evaporation. A shadow mask was used to create eight 4 mm^2 pixels. Devices were fabricated and encapsulated in a nitrogen glovebox. Hole-only diodes were prepared as described above; however gold was used for the top contact rather than aluminum.

Acknowledgment. We thank C. Groves for useful discussions, Cambridge Display Technology Ltd. for supplying the polymers F8BT, PFB, and F8TBT, and the EPSRC for financial support. R.A.M. thanks the Schiff foundation, I.A.H. thanks the Cambridge Commonwealth Trust and S.W. thanks Fitzwilliam College Cambridge and the Swedish Research Council for financial support.

References

(1) Halls, J. J. M.; Walsh, C. A.; Greenham, N. C.; Marseglia, E. A.; Friend, R. H.; Moratti, S. C.; Holmes, A. B. *Nature* **1995**, *376*, 495.
(2) Yu, G.; Gao, J.; Hummelen, J. C.; Wudl, F.; Heeger, A. J. *Science* **1995**, *270*, 1789.
(3) McNeill, C. R.; Abrusci, A.; Zaumseil, J.; Wilson, R; McKiernan, M. J.; Burroughes, J. H.; Halls, J. J. M; Greenham, N. C.; Friend, R. H. *Appl. Phys. Lett.* **2007**, *90*, 193506.
(4) Kim, J. Y.; Lee, K.; Coates, N. E.; Moses, D.; Nguyen, T.-Q.; Dante, M.; Heeger, A. J. *Science* **2007**, *317*, 222.
(5) McNeill, C. R.; Westenhoff, S; Groves, C.; Friend, R.; Greenham, N. C. *J. Phys. Chem. C* **2007**, *111*, 19153.
(6) Mandoc, M. M.; Veurman, W.; Sweelssen, J.; Koetse, M. M.; Blom, P. W. M. *Appl. Phys. Lett.* **2007**, *91*, 073518.
(7) Forrest, S. R. *Nature* **2004**, *428*, 911.
(8) Padinger, F; Rittberger, R. S.; Sariciftci, N. S. *Adv. Funct. Mater.* **2003**, *13*, 85.
(9) Zhao, Y.; Xie, Z.; Qu, Y.; Geng, Y.; Wang, L. *Appl. Phys. Lett.* **2007**, *90*, 043504.
(10) Arias, A. C.; Corcoran, N.; Banach, M.; Friend, R. H.; MacKenzie, J. D.; Huck, W. T. S. *Appl. Phys. Lett.* **2002**, *80*, 1695.
(11) Zhang, F.; Jespersen, K. G.; Björström, C.; Svensson, M.; ersson, M. R.; Sundström, V.; Magnusson, K.; Moons, E.; Yartsev, A.; Inganäs, O. *Adv. Funct. Mater.* **2006**, *16*, 667.
(12) Peet, J.; Kim, J. Y.; Coates, N. E.; Ma, W. L.; Moses, D.; Heeger, A. J.; Bazan, G. C. *Nat. Mater.* **2007**, *6*, 497.
(13) Lee, J. K.; Ma, W. L.; Brabec, C. J.; Yuen, J; Moon, J. S.; Kim, J. Y.; Lee, K.; Bazan, G. C.; Heeger, A. J. *J. Am. Chem. Soc.* **2008**, *130*, 3619.
(14) Halls, J. J. M.; Arias, A. C.; MacKenzie, J. D.; Weishi, W.; Inbasekaran, M.; Woo, E. P.; Friend, R. H. *Adv. Mater.* **2000**, *12*, 7–498.
(15) Arias, A. C.; MacKenzie, J. D.; Stevenson, R.; Halls, J. J. M.; Inbasekaran, M.; Woo, E. P.; Richards, D.; Friend, R. H. *Macromolecules* **2001**, *34*, 17–6005.
(16) Stevens, M. A.; Silva, C; Russell, D. M.; Friend, R. H. *Phys. Rev. B* **2001**, *63*, 165213.
(17) Chirvase, D.; Parisi, J.; Hummelen, J. C.; Dyakonov, V. *Nanotechnology* **2004**, *15*, 1317.
(18) Miller, S.; Fanchini, G.; Lin, Y.-Y.; Li, C.; Chen, C.-W.; Su, W.-F.; Chhowalla, M. *J. Mater. Chem.* **2008**, *18*, 306.
(19) de Mello, J. C.; Wittmann, H. F.; Friend, R. H. *Adv. Mater.* **1997**, *9*, 230.
(20) Westenhoff, S.; Howard, I. A.; Friend, R. H. *Phys. Rev. Lett.* **2008**, *101*, 016102.
(21) Stevens, M. A.; Silva, C.; Russell, D. M.; Friend, R. H. *Phys. Rev. B* **2001**, *63*, 165213.
(22) Westenhoff, S.; Howard, I. A.; Hodgkiss, J. M. *J. Am. Chem. Soc.*, in press
(23) Mihailetchi, V. D.; Koster, L. J. A.; Hummelen, J. C.; Blom, P. W. M. *Phys. Rev. Lett.* **2004**, *93*, 216601.
(24) De, S.; Pascher, T.; Maiti, M.; Jespersen, K. G.; Kesti, T.; Zhang, F.; Inganas, O.; Yartsev, A.; Sundstrom, V. *J. Am. Chem. Soc.* **2007**, *129*, 27–8466.
(25) Marsh, R. A.; McNeill, C. R.; Abrusci, A.; Campbell, A. R.; Friend, R. H. *Nano Lett.* **2008**, *8*, 1393.
(26) Marsh, R. A.; Groves, C.; Greenham, N. C. *J. Appl. Phys.* **2007**, *101*, 083509.
(27) Okhita, H.; Cook, S.; Astuti, Y.; Duffy, W.; Tierney, S.; Zhang, W.; Heeney, M.; McCulloch, I.; Nelson, J.; Bradley, D. D. C.; Durrant, J. R. *J. Am. Chem. Soc.* **2008**, *130*, 3030–3042.
(28) Groves, C.; Marsh, R. A.; Greenham, N. C. *J. Phys. Chem.* **2008**, *129*, 114903.
(29) Brown, P. J.; Thomas, D. S.; Köhler, A.; Wilson, J.; Kim, J.-S.; Ramsdale, C. M.; Sirringhaus, H; Friend, R. H. *Phys. Rev. B* **2003**, *67*, 064203.
(30) Erb, T.; Zhokhavets, U.; Gobsch, G.; Raleva, S.; Stuhn, B.; Schilinsky, P.; Waldauf, C.; Brabec, C. J. *Adv. Funct. Mater.* **2005**, *15*, 1193.
(31) Murgatroyd, P. N. *J. Phys. D* **1970**, *3*, 151.

NL802425R